PNAS RESEARCH ARTICLE | PLANT BIOLOGY

RALF1 peptide triggers biphasic root growth inhibition upstream of auxin biosynthesis

Lanxin Li[a,b], Huihuang Chen[b], Saqer S. Alotaibi[c], Aleš Pěnčík[d], Maciek Adamowski[b], Ondřej Novák[d], and Jiří Friml[b,1]

Edited by Natasha Raikhel, Center for Plant Cell Biology, Riverside, CA; received November 19, 2021; accepted June 13, 2022

Plant cell growth responds rapidly to various stimuli, adapting architecture to environmental changes. Two major endogenous signals regulating growth are the phytohormone auxin and the secreted peptides rapid alkalinization factors (RALFs). Both trigger very rapid cellular responses and also exert long-term effects [Du *et al., Annu. Rev. Plant Biol.* 71, 379–402 (2020); Blackburn *et al., Plant Physiol.* 182, 1657–1666 (2020)]. However, the way, in which these distinct signaling pathways converge to regulate growth, remains unknown. Here, using vertical confocal microscopy combined with a microfluidic chip, we addressed the mechanism of RALF action on growth. We observed correlation between RALF1-induced rapid *Arabidopsis thaliana* root growth inhibition and apoplast alkalinization during the initial phase of the response, and revealed that RALF1 reversibly inhibits primary root growth through apoplast alkalinization faster than within 1 min. This rapid apoplast alkalinization was the result of RALF1-induced net H^+ influx and was mediated by the receptor FERONIA (FER). Furthermore, we investigated the cross-talk between RALF1 and the auxin signaling pathways during root growth regulation. The results showed that RALF-FER signaling triggered auxin signaling with a delay of approximately 1 h by up-regulating auxin biosynthesis, thus contributing to sustained RALF1-induced growth inhibition. This biphasic RALF1 action on growth allows plants to respond rapidly to environmental stimuli and also reprogram growth and development in the long term.

RALF1 | auxin | cross-talk | root growth inhibition | biphasic regulation

Significance

Regulation of growth is crucial for overall plant development and its adaptation to environment. Peptide rapid alkalinization factors 1 (RALF1) and phytohormone auxin are key growth regulators with characteristic both rapid and long-term effects. However, the underlying mechanism and coordination of these signals are unclear. Our study reveals that those two signals trigger rapid growth inhibition (<1 min) by rapidly alkalinizing the apoplast, a result of rapid net H^+ influx across the plasma membrane; nonetheless, their signaling mechanisms are independent. RALF1 sustains root growth inhibition long term by inducing auxin biosynthesis and signaling. These discoveries contribute to the understanding of rapid plant growth responses and hormone-peptide cross-talk for optimization of plant growth and architecture also relevant for agriculture applications.

Plant motions and growth adaptations occur at different time scales, from seed bursting in milliseconds to stomata opening in minutes to long-term architecture adaptation. One of the fastest underlying cellular motions is water-driven cell growth, such as root cell expansion under abiotic or biotic stress or during gravitropism. Cell growth is directly regulated by the apoplastic pH, according to the Acid Growth Theory (1,2), which states that a low pH activates enzymatic reactions to modify the extensibility of cell walls and promote cell growth. Among numerous plant growth regulators, two recognized endogenous signals impacting on rapid cell growth are rapid alkalinization factor (RALF) peptides and the phytohormone auxin.

The RALF1 polypeptide can dramatically arrest root growth and alkalinize the cell medium (3, 4). It belongs to a family of over 37 members in *Arabidopsis thaliana* (5, 6). The presence of RALFs throughout the plant kingdom (as well as in fungi and bacteria) indicates their importance in the fundamental regulatory processes of plant growth and development (7, 8). The first discovered RALF receptor, FERONIA (FER), belongs to the *Catharanthus roseus* RLK1-like (crRLK1L) family in *A. thaliana*, with 17 members (9, 10). FER is located in the plasma membrane (PM) and consists of an extracellular domain with two malectin-like domains, a transmembrane domain, and an intracellular kinase domain (11). The kinase domain partially contributes to RALF1-induced root growth inhibition (12, 13).

RALF1-induced extracellular alkalinization coincides with RALF1-triggered phosphorylation of the PM H^+-ATPase 2 (AHA2) at Ser899 (9). Phosphomimetic mutation AHA2 S899D in yeast causes yeast cell growth inhibition (9). Thus, AHA H^+ pumps are thought to mediate RALF1-induced growth inhibition. However, whether H^+ pump activity is reduced by RALF1 and how this contributes to RALF1-FER–mediated alkalinization remain largely unknown (14). Moreover, several studies have shown that some RALF1-elicited growth inhibition might be independent of alkalinization (15, 16), leaving the biological roles of the RALF1-induced apoplastic pH increase and other downstream effects of RALF1 signaling an open question (14).

Unlike RALFs, auxin is a long-range endogenous signal (17). Natural auxin, indole-3-acetic acid (IAA), is synthesized in both shoots and roots. It is mainly derived from the amino acid tryptophan (Trp) after sequential catalysis by the Trp aminotransferase of *Arabidopsis* (TAA) family and the YUCCA (YUC) family (18). Auxin can then be

Author contributions: L.L. and J.F. designed research; L.L. and H.C. performed research; A.P. and O.N. performed the auxin metabolites experiments; L.L. and H.C. analyzed data; L.L. and J.F. wrote the paper; and S.S.A. and M.A. revised the manuscript.

The authors declare no competing interest.

This article is a PNAS Direct Submission.

[1]To whom correspondence may be addressed. Email: jiri.friml@ist.ac.at.

This article contains supporting information online at http://www.pnas.org/lookup/suppl/doi:10.1073/pnas.2121058119/-/DCSupplemental.

Published July 25, 2022.

directionally transported from cell to cell via PIN, AUX1/LAX, and ABCB transporters (19). Finally, auxin participates in several signaling pathways. The TIR1/AFB receptors mediate the nuclear auxin signaling pathway together with the coreceptors Aux/IAA for transcriptional regulation (20). The TIR1/AFB receptors have also been shown to mediate a rapid, nontranscriptional net H^+ influx across the PM for rapid growth inhibition (21–23). Moreover, the transmembrane kinase (TMK) family (auxin signaling components on the cell surface) plays versatile roles in growth regulation. TMK1 regulates gene transcription in the apical hook (24) and phosphorylates and activates PM H^+-ATPases, leading to apoplast acidification and growth promotion in shoots and roots (23, 25). TMK4 suppresses auxin biosynthesis (26). Auxin biosynthesis, transport, and signaling collectively contribute to the regulation of cell growth.

Both RALF and auxin trigger rapid responses, including extracellular alkalinization and growth inhibition. The cross-talk between these two growth regulators is of great interest. FER possibly plays a role in auxin-regulated root growth inhibition (27). Conversely, RALF1-FER signaling regulates auxin transport. For example, *fer-4* mutants have aberrant PIN2 and AUX1 polarity during gravitropism and root nutation growth (28, 29). Moreover, RALF1 has been found to trigger PIN2 internalization (30). Despite their connections, the way in which these two growth regulators converge in the immediate responses of extracellular alkalinization and primary root growth inhibition and their long-term effects remain largely unknown.

In this study, we addressed the mechanism of RALF-induced growth regulation and its connection to auxin signaling. We revealed that RALF and auxin signaling independently converge on rapid apoplast alkalinization and root growth inhibition, whereas for the sustained growth attenuation, RALF through its receptor FER induces auxin biosynthesis and signaling.

Results

RALF1 and Auxin Alkalinize the Apoplast to Inhibit Root Growth Rapidly and Reversibly. RALF1 induces rhizosphere alkalinization (31) and dramatically inhibits root growth (14). The rapid action of RALF1 resembles that of auxin, which also triggers apoplast alkalinization, leading to root growth inhibition within 30 s (23). To examine the temporal dynamics of RALF1-regulated root growth and the causal relationship between RALF1-induced alkalinization and growth inhibition, we used a microfluidic vRootchip (21, 23) combined with vertical confocal microscopy (32) for live imaging and applied a membrane-impermeable ratio-metric pH dye, 8-hydroxypyrene-1,3,6-trisulfonic acid (HPTS) (27) to investigate changes in the apoplastic pH. We tracked root tip growth as a sensitive readout for the accumulative effects of the elongation of individual cells and simultaneously monitored the apoplastic pH in elongated cells. We found that externally applied RALF1 at 10 μM dramatically inhibited root tip growth (Fig. 1*A*) and alkalinized the apoplast in elongated cells (Fig. 1*B*) within 1 min of application (Fig. 1*C*), indicating a close correlation between apoplast alkalinization and root growth inhibition induced by RALF1. As a complementary approach, we analyzed the cytosolic pH in the elongated epidermal cells using a PM-Cyto reporter (33). The cytosolic pH adjacent to the PM decreased rapidly after RALF1 application (Fig. 1*D*). The pH increases outside the PM and the decreases inside it suggest that RALF1 triggers a rapid net H^+ influx into the cell, in line with previous observations of RALF33- and RALF36-induced increase in H^+ net flux measured by a noninvasive microelectrode (34).

Rapid growth responses to auxin occur without a need of transcriptional regulation (21, 23). We thus examined whether this applies to RALF1 as well. We applied the protein translation inhibitor cycloheximide for 3 min in vRootchip to block protein synthesis (21). We found that the addition of RALF1 still led to rapid root growth inhibition and apoplast alkalinization (*SI Appendix*, Fig. S1*A*), suggesting that RALF1 nontranscriptionally regulates a rapid net H^+ influx and root growth inhibition. Furthermore, we examined whether RALF1-induced growth inhibition is reversible, like the response to auxin (21). We attempted to wash out the RALF1 effect using the basal medium in vRootchip; however, there was no growth recovery, and RALF1 precipitation blocked the medium flow in vRootchip within hours. Employing an alternative method, we transferred RALF1-pretreated seedlings to a fresh agar block containing a basal medium and observed a complete recovery of growth within 20 min (*SI Appendix*, Fig. S1*B*). This suggests that RALF1 inhibits root growth and alkalinizes the apoplast rapidly and reversibly.

FER Receptor Mediates RALF1 Effect on Apoplast Alkalinization and Root Growth Inhibition. To examine whether FER, the receptor of RALF1 on the PM (30), mediated the RALF1-triggered rapid responses, we analyzed *fer-4* mutants in vRootchip. After the application of 5 μM of RALF1, we observed that *fer-4* mutants were almost insensitive in rapid growth inhibition as compared to both WT and the complemented *pFER::FER-GFP/fer-4* (Fig. 1*E* and *SI Appendix*, Fig. S1*C*), and in apoplast alkalinization as compared to the WT (Fig. 1*F*). These suggest that FER contributes to RALF1-triggered rapid responses, consistent with previous studies showing that FER mediates the rapid net H^+ influx induced by RALF33 (34) and the long-term medium pH changes triggered by RALF1 (9). To track the long-term growth response, we recorded seedlings transferred to media containing various concentrations of RALF1 on a high-throughput vertical scanner (35). We found that the *fer-4* mutants were completely insensitive to 0.1 to 10 μM of RALF1 (*SI Appendix*, Fig. S1 *D* and *E*) from the first to the fifth hour, indicating that FER mediates long-term growth responses. To examine whether other FER paralogs from the RLK family contribute to RALF1-mediated long-term growth inhibition, we analyzed the root growth of *the1-1* and *herk1-1* mutants after RALF1 treatment at various concentrations. We found that all of them exhibited a normal growth response over time (*SI Appendix*, Fig. S1 *D*, *F*, and *G*). Overall, FER dominantly mediates RALF1-triggered rapid and long-term growth inhibition.

RALF1-triggered rapid root growth inhibition and apoplast alkalinization closely correlate over time (Fig. 1*A*–*C*). As we showed previously, in the context of auxin-triggered root growth, manipulation with the medium's pH has a direct impact on root growth (23). We observed that an alkaline medium alkalinized apoplast and inhibited root growth, while an acidic medium acidified apoplast and promoted growth immediately and reversibly (Fig. 1*G*–*J*), suggesting that RALF1-triggered apoplastic alkalinization caused rapid root growth inhibition. Importantly, *fer-4*, WT, and the complemented line had similar responses to external pH manipulation (Fig. 1*G*–*J* and *SI Appendix*, Fig. S1 *H* and *I*), indicating that FER does not sense or respond to pH fluctuations but mediates RALF1-induced rapid apoplastic alkalinization and root growth inhibition.

Auxin Action on Growth Inhibition Does Not Require RALF-FER. The RALF-FER and auxin-TIR1/AFB signaling mechanisms (23) have very similar rapid effects on cellular net H^+ influx and root growth inhibition. To investigate the possible interdependence of these mechanisms, we reciprocally examined the

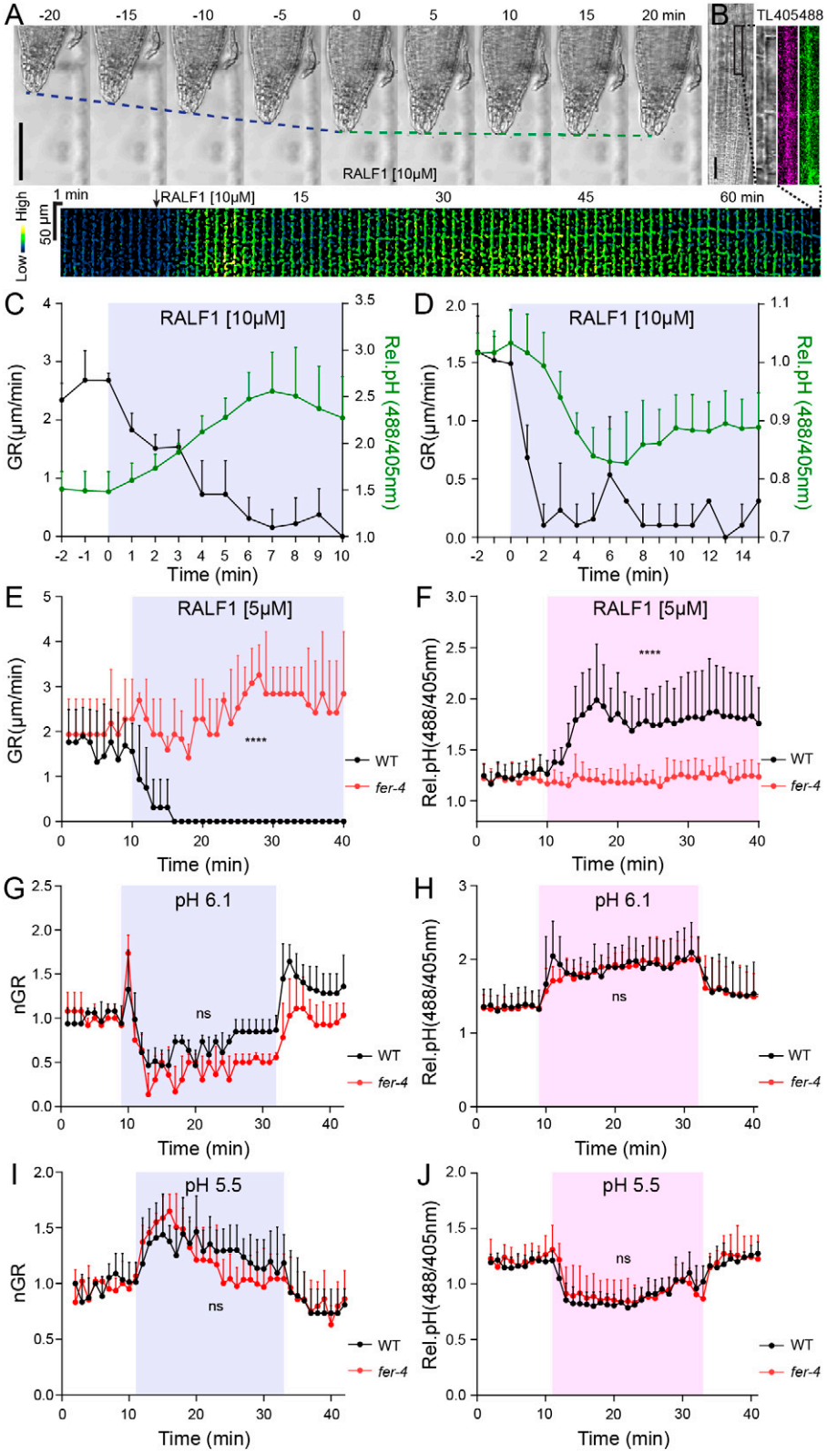

Fig. 1. RALF1-FER signaling mediates rapid apoplast alkalinization correlating with rapid growth inhibition. (*A*) Time-lapse of root growth response to 10 μM RALF1 in vRootchip. The slope of blue and green dotted lines that track the root tip indicates the growth rate (GR) in basal medium and RALF1 medium, respectively. (Scale bar, 100 μm.) (*B*) Time lapse of apoplastic pH response in root tip epidermal cells to 10 μM RALF1 in vRootchip. pH was monitored in the same ROI for 85 min by the ratiometric HPTS dye. The image represents the ratio of emissions upon excitation at 488 and 405 nm. ROI includes root elongating cells. TL is transmitted light image. (Scale bar, 50 μm.) (*C*) Quantification of root GR (*A*) and apoplastic pH in elongating cells (*B*) of WT plants with RALF1 treatment in vRootchip. Mean of four roots + SD. (*D*) Root growth and cytosolic pH in elongating cells of WT plants with 10 μM RALF1 treatment in vRootchip. Mean of three roots + SD. Cytosolic pH was quantified using the PM-Cyto marker. (*E* and *F*) Root GR and apoplastic pH in *fer-4* and WT responding to 5 μM RALF1 treatment in vRootchip. Mean of four roots for WT and three for *fer-4* + SD (*E*). Mean of four roots for WT and *fer-4* + SD (*F*). ****$P < 0.0001$, two-way ANOVA. (*G–J*) Normalized root growth (nGR) (*G* and *I*) and apoplastic pH (*H* and *J*) in *fer-4* and WT in response to a pulse of alkaline (pH 6.1) (*G* and *H*) or acidic (pH 5.5) (*I* and *J*) medium. nGR were normalized to the average value of the same genotype before treatment. Mean of three roots for *fer-4* and WT + SD (*G*). Mean of three roots for WT and five for *fer-4* + SD (*H*). Mean of five roots for WT and three for *fer-4*+SD (*I*). Mean of four roots for WT and *fer-4* + SD (*J*). ns, $P > 0.05$, two-way ANOVA. The shaded areas represent the duration of the indicated treatments.

root growth response of the mutants in one pathway to the ligand of the other. In vRootchip, *fer-4* showed rapid and normal growth inhibition after treatment with 5 nM of IAA (*SI Appendix*, Fig. S2*A*). Using the vertical scanner, we also observed that IAA inhibited the root growth of *fer-4*, *the1-1*, and *herk1-1* mutants similarly to WT over a period of 6 h (*SI Appendix*, Fig. S2*B*). Only when we used a high dose of IAA (100 nM) did we observe a transient and slight growth resistance of *fer-4* mutants, and only between the first and fifth hours (*SI Appendix*, Fig. S2 *C* and *D*), in line with a previous study reporting *fer-4* resistance to 250 nM of IAA after 8 h of incubation (27). We think that this transient nature of decreased sensitivity and the high level of auxin required could be due to deficient auxin uptake caused by defective polarity of the PIN2 auxin transporter in *fer-4* mutants (28, 29). Overall, we did not find evidence of a direct role of FER and its paralogs in auxin-mediated root growth inhibition for the time scale of 0 to 6 h in our study.

RALF-FER Action on Growth Inhibition Does Not Require TMK or AHA Activity. Reciprocally, we examined whether auxin signaling is required for the RALF1-triggered growth inhibition. First, we analyzed the contribution of the cell surface auxin signaling components TMK. Because *tmk1,4* mutants grow too slowly to detect rapid changes, we chose *tmk1,2* mutants that display the strongest phenotype of the remaining *tmk* mutant combinations (23). In vRootchip, the growth of *tmk1,2* roots was as strongly inhibited by RALF1 as WT roots, while the apoplast was significantly more alkalinized in *tmk1,2* after RALF1 (*SI Appendix*, Fig. S3 *A* and *B*). This does not support role of TMK in mediating RALF1-induced alkalinization, but rather hints at a possible antagonistic effect. Accordingly, *tmk1,2* roots displayed a hypersensitivity in accumulated growth inhibition after treatment with RALF1 for 1 to 5 h (*SI Appendix*, Fig. S3 *C* and *D*). In addition, *tmk1-1* and *tmk1,4* roots showed a trend of hypersensitivity to RALF1, while *tmk4-1* responded normally (*SI Appendix*, Fig. S3 *C* and *E–G*). These suggest that this branch of auxin signaling is not directly involved in RALF1-mediated root growth inhibition.

Notably, previous studies have shown that *tmk* mutants have a significantly reduced abundance of AHA2 and general H^+-ATPase activity (23, 25). Given that *tmk* mutants exhibit a normal or even hypersensitive response to RALF1, this suggests that H^+-ATPases do not contribute to RALF1-induced growth inhibition. We tested this directly by assessing growth responses to RALF1 in *aha* mutants. For the rapid responses, we tested in vRootchip a knockdown line, *AtTAS1c-AHA*, expressing synthetic transacting small-interfering RNA (siRNA) (36) targeting *AHA1/2/7/11* under the *PIN2* promoter in the outer root tissues (23). We found that *AtTAS1c-AHA#4* had normal rapid responses to RALF1 (*SI Appendix*, Fig. S3 *H* and *I*). For a longer-term response, we analyzed the growth of available mutants by scanner. The single mutants *aha1-6* and *aha2-4* showed normal responses to 5 μM of RALF1 in terms of growth inhibition(*SI Appendix*, Fig. S3*J*). Notably, the knockdown *AtTAS1c-AHA* lines showed hypersensitivity to 5 μM of RALF1, in line with the hypersensitivity in *tmk* mutants (*SI Appendix*, Fig. S3*K*). The hyperactive *ost2-3D* mutants and *35S::SAUR19-GFP* lines with constitutively active AHAs (37) responded normally to 5 μM of RALF1 (*SI Appendix*, Fig. S3*L*).

Although we cannot exclude the residual activity in all mutants above, the observations do not support TMK and AHA involvement in RALF1-induced growth inhibition for the time scale of 0 to 6 h. It requires further examination whether RALF signaling opens an unknown H^+ channel or transporter mediating net H^+ influx across the PM, similar as has recently been suggested for auxin-induced apoplast alkalinization via TIR1/AFB signaling (23).

Sustained RALF-FER Action on Growth Inhibition Requires TIR1/AFB-Aux/IAA-ARF Signaling. Next, we investigated the involvement of the TIR1 auxin signaling in RALF1-induced root growth inhibition. We analyzed the *tir triple* mutants in vRootchip and observed no significant difference from WT in growth inhibition and apoplast alkalinization after 5 μM of RALF1 for 50 min (Fig. 2*A* and *B*). To further test the role of the TIR1/AFB pathway in RALF-induced growth inhibition in a high-throughput manner, we tracked growth dynamics every 1 h by vertical scanner. We employed the synthetic compound PEO-IAA [2-(1H-Indol-3-yl)-4-oxo-4-phenyl-butyric acid], which acts as an auxin antagonist and blocks TIR1/AFB-mediated signaling by binding to the TIR1/AFB receptors (38). Notably, the application of 10 μM of PEO-IAA rescued root growth inhibition caused by 5 μM of RALF1, with the effect becoming stronger after approximately 1 h (Fig. 2*C* and *D*). Additionally, we employed a dominant-negative variant of the Aux/IAA protein IAA17, expressed conditionally in the *HS::axr3-1* line. After heat-shock induction, *HS::axr3-1* seedlings exhibited reduced sensitivity to root growth inhibition at 5 μM of RALF1 after 1 h (Fig. 2*E*). These results indicate that TIR1/AFB-mediated auxin signaling participates in RALF1-induced long-term root growth inhibition.

Thus, blocking the TIR1/AFB pathway made roots resistant to RALF1-triggered root growth inhibition after approximately 1 h, while they seemed to be less affected at early time points. As RALF peptides precipitate over time and block the channels in the vRootchip, we tried to reveal the dynamics with the temporal resolution overlapping the vRootchip and vertical scanner. We performed confocal imaging after transferring samples to agar blocks containing treatments and automatically tracked the root tip over time using TipTracker, a MATLAB-based program (32). We observed that the *tir triple* mutants showed normal growth reduction after treatment with 2 μM of RALF1 in the first hour but subsequently started to show resistance, increasing the growth rate, recovering to more than 80% of the initial rate after five hours (Fig. 2*F*). Consistently, after treatment with 2 μM of RALF1, the apoplast pH in the WT and *tir triple* increased to a similar extent in the first hour, after which the pH kept increasing in the WT but not in *tir triple* (Fig. 2*G*). This indicates that the auxin signaling mutant *tir triple* exhibits a biphasic response to RALF1 treatment: its initial response is as sensitive as that of the WT, but its sensitivity decreases in the long term. This suggests a role of TIR/AFB signaling in the latter phase of the RALF1 response. We next examined whether the biphasic RALF1 response depended on the RALF1 dosage. We analyzed the growth responses to RALF1 at concentrations ranging from 1 to 5 μM on the vertical scanner. We observed a biphasic growth response in *tir triple* at 3 and 5 μM of RALF1, whereas 1 and 2 μM were not effective (*SI Appendix*, Fig. S4). The growth rate of the mutants started to recover from 40 min onward, in line with the confocal imaging result (Fig. 2*F*).

Taking these data together, we find that RALF1-mediated biphasic growth responses in auxin signaling–deficient roots, either in mutants or after pharmaceutical manipulations, indicate that RALF1 plays a bimodal growth regulatory role and that auxin signaling is required for the sustained growth reduction after the initial, FER-mediated, response.

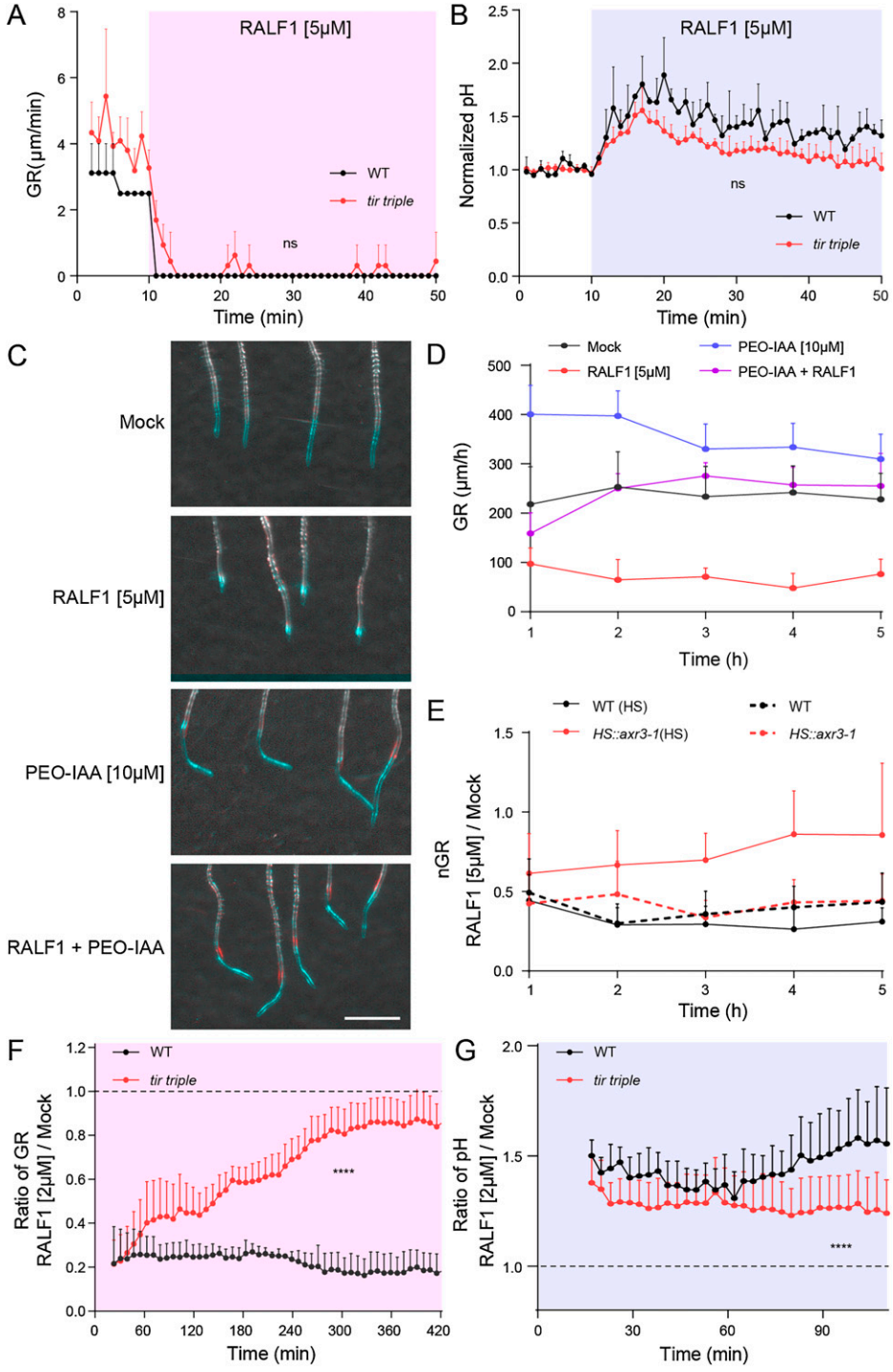

Fig. 2. TIR1/AFB auxin signaling is downstream of RALF1-FER pathway during sustained root growth inhibition. (*A* and *B*) Root GR (*A*) and normalized apoplastic pH (*B*) in *tir triple* and WT with RALF1 treatment in vRootchip. Normalized pH was normalized to the average value of the same genotype before treatment. Mean of two roots for WT and 4 for *tir triple* + SD (*A* and *B*). ns, $P > 0.05$, two-way ANOVA. (*C* and *D*) Visualization (*C*) and quantification (*D*) of root GR in WT plants on vertical scanner after 5 μM RALF1 treatment with or without 10 μM PEO-IAA. Plants were preincubated in PEO-IAA or Mock treatment for 80 min. Images at 0 h (red) and 5 h (cyan) were merged; white pixels represent the coincided area of two time points, and cyan and red indicates the part which is absent in the other time point. (Scale bar, 2 mm) (*C*). $n > 9$, mean + SD. $P < 0.0001$ between RALF1 and PEO-IAA+RALF1, two-way ANOVA (*D*). (*E*) nGR in *HS::axr3-1* and WT on vertical scanner. nGR is growth rate after 5 μM RALF1 normalized by that on Mock treatment corresponding to the same time points. Dotted lines are samples without heat shock induction. $n > 11$, mean + SD. $P < 0.0001$ between heat-shocked *HS::axr3-1* and heat-shocked WT. (*F* and *G*) Ratio of GR (*F*) and apoplastic pH (*G*) of *tir triple* and WT on vertical confocal microscopy. The ratio is calculated as GR or apoplastic pH after RALF1 treatment normalized by that after Mock corresponding to the same time points (*D*). $n > 6$, mean + SD. ****$P < 0.0001$, two-way ANOVA for both graphs. The shaded areas represent the duration of the indicated treatments.

RALF1-FER Signaling Triggers TIR1/AFB-Mediated Auxin Signaling. To further verify that the auxin-TIR1/AFB signaling pathway is downstream of RALF1-FER during root growth inhibition, we tracked the output of canonical auxin signaling using the *R2DII* reporter, which is based on the auxin-triggered degradation of the auxin-responsive DII domain of Aux/IAA (39). Treatment with RALF1 at 10 μM led to DII degradation similarly to the effect of auxin at 10 nM, but with a slower kinetics

(Fig. 3*A*). This indicates that RALF1 triggers nuclear auxin signaling. This RALF1-induced DII degradation was rescued by pretreatment with 10 μM of PEO-IAA (Fig. 3*B* and *C*). In addition, we compared the kinetics of auxin signaling activation induced by RALF1 and IAA using the *DR5::LUC* line (40), in which the synthetic auxin-responsive promoter DR5 drives the expression of a fast folded/active luciferase enzyme. We found that 10 μM of RALF1 triggered significant auxin signaling with a delay of ∼10 min compared to treatment with 5 nM IAA (Fig. 3*D* and *E*). These observations suggest that RALF1 indirectly induces auxin canonical TIR1/AFB signaling and that this TIR1/AFB auxin signaling in turn inhibits root growth mediates RALF1-FER–induced, sustained root growth inhibition.

We next examined whether the canonical TIR1/AFB auxin signaling pathway is also involved in root growth inhibition mediated by other RALF peptides. We analyzed RALF22, which, like RALF1, belongs to clade I of the RALF peptides (5). RALF22 inhibited root growth from the first hour onward and exerted a dosage-dependent effect similar to that of RALF1 (*SI Appendix*, Fig. S5*A*). The application of 10 μM of RALF22 led to DII degradation (*SI Appendix*, Fig. S5*B*) and an increase in DR5rev::GFP (*SI Appendix*, Fig. S5*C*) as well as DR5::LUC signal with a delay of ∼10 min compared to 5 nM of IAA (*SI Appendix*, Fig. S5*D*). Furthermore, the *tir triple* mutants became resistant to growth inhibition at 10 μM of RALF22 after 1 h, whereas *tmk1-1* mutants exhibited a normal growth response (*SI Appendix*, Fig. S5*E*). These observations indicate that TIR1/AFB-mediated auxin signaling is broadly involved in root growth inhibition induced by RALF peptides.

RALF1-FER Signaling Induces Auxin Biosynthesis. The above results show that auxin signaling participates in RALF1-induced sustained root growth inhibition. Two major scenarios may explain how RALF1-FER signaling triggers auxin signaling with a characteristic delay: the regulation of auxin transport and the regulation of auxin biosynthesis. We addressed this question using pharmacological and genetic approaches. We pretreated seedlings with auxin transport inhibitors *N*-1-naphthylphthalamic acid (NPA) and 2,3,5-triiodobenzoic acid (TIBA) (41) at 10 μM for 80 min and then applied 5 μM of RALF1 in a cotreatment with these inhibitors. We observed no rescue of RALF1-induced root growth inhibition (*SI Appendix*, Fig. S6 *A* and *B*). We also tested the effect of RALF1 on mutants of *PIN* auxin efflux transporters *pin2* and *pin3,4,7*. Both mutants reacted normally to treatment with RALF1 at different concentrations (*SI Appendix*, Fig. S6*C*). These observations do not support a modulation of auxin transport as the mechanism, by which RALF1 triggers auxin signaling for root growth inhibition.

To examine whether RALF1 signaling inhibits root growth via auxin biosynthesis, we preincubated seedlings in auxin biosynthesis inhibitors L-kynurenine (KYN; 20 μM) and yucasin (YUCA; 25 μM) (42, 43) for 80 min and then evaluated root growth on the surface of media additionally supplemented with 5 μM of RALF1. We observed that KYN completely rescued RALF1-mediated root growth inhibition after 4 h (Fig. 4*A*), while YUCA resulted in partial rescue (Fig. 4*B*). Similarly, KYN fully rescued RALF1-induced DII degradation, while YUCA had a partial effect (*SI Appendix*, Fig. S7 *A* and *B*). Additionally, we tested the mutants of auxin biosynthesis genes *TAA1*, *TAR1*, *TAR2*, and *YUCCA*s (44)—including *wei8-1tar2-2*, *wei8-3tar2-2*, *wei8-3tar2-1*, *wei8-3tar1-1*, and *yuc2,5,7,8*—and found that they were partially resistant to root growth inhibition at 5 μM of RALF1 (Fig. 4*C* and *D*). These observations strongly suggest that auxin biosynthesis is involved in RALF1-triggered sustained root growth inhibition. As elevated auxin levels inhibit root growth (23),

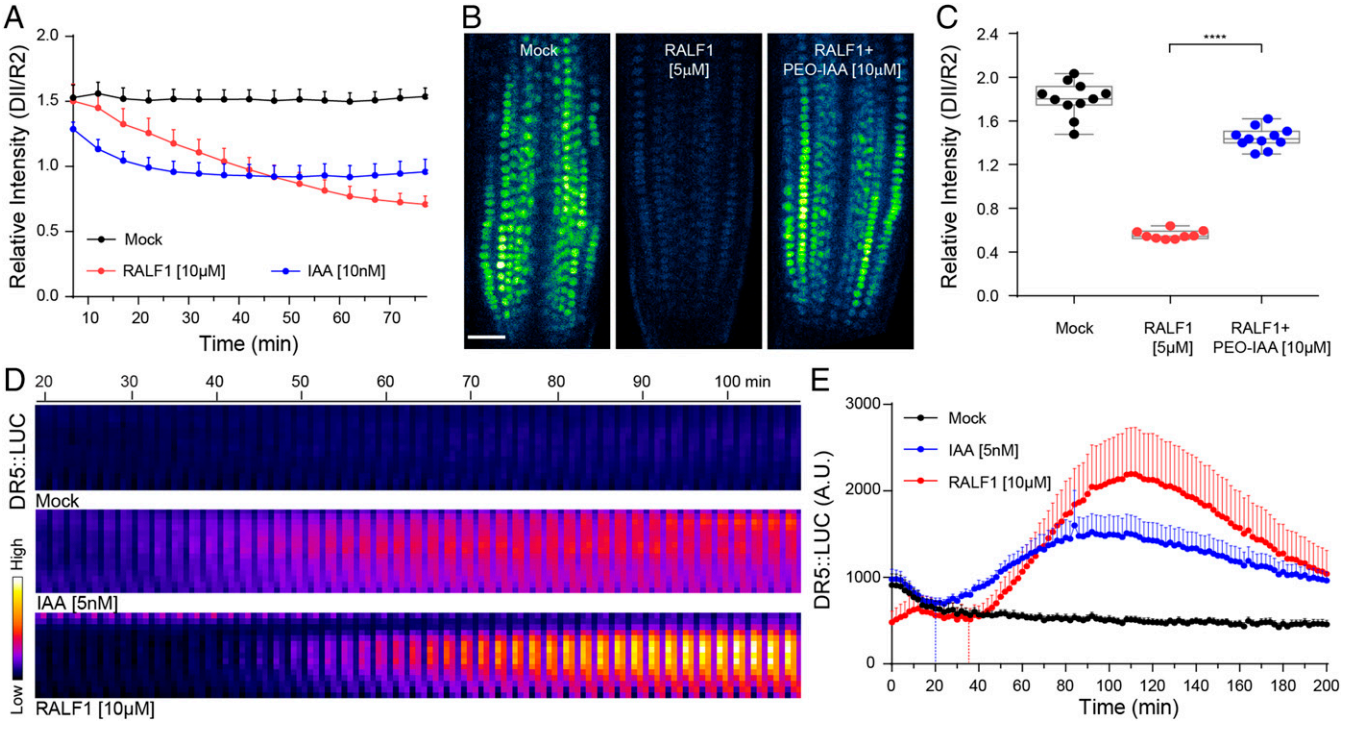

Fig. 3. RALF1 triggers auxin signaling (*A*) Normalized fluorescence intensity of the AUX/IAA DII domain after treatment with 10 μM RALF1, 10 nM IAA, or Mock. $n > 9$, mean + SD. (*B* and *C*) Visualization of DII (*B*) and quantification of normalized DII intensity (*C*) after 5 μM RALF1 treatment for 160 min with pretreatment of 10 μM PEO-IAA or Mock for 80 min. Green-Fire-Blue LUT was applied. (Scale bar, 30 μm.) (*B*). Box plot bars show the minimum and maximum value. $n > 9$ for each condition, ****$P < 0.0001$, one-way ANOVA (*C*). (*D* and *E*) Time lapse (*D*) and quantification (*E*) of DR5::LUC signal in root tip after treatment with 5 nM IAA, 10 μM RALF1 or Mock. Fire LUT was applied (*D*). Dotted lines indicate the time points at which signal intensity started to increase; $n > 6$ for each condition, mean + SD (*E*).

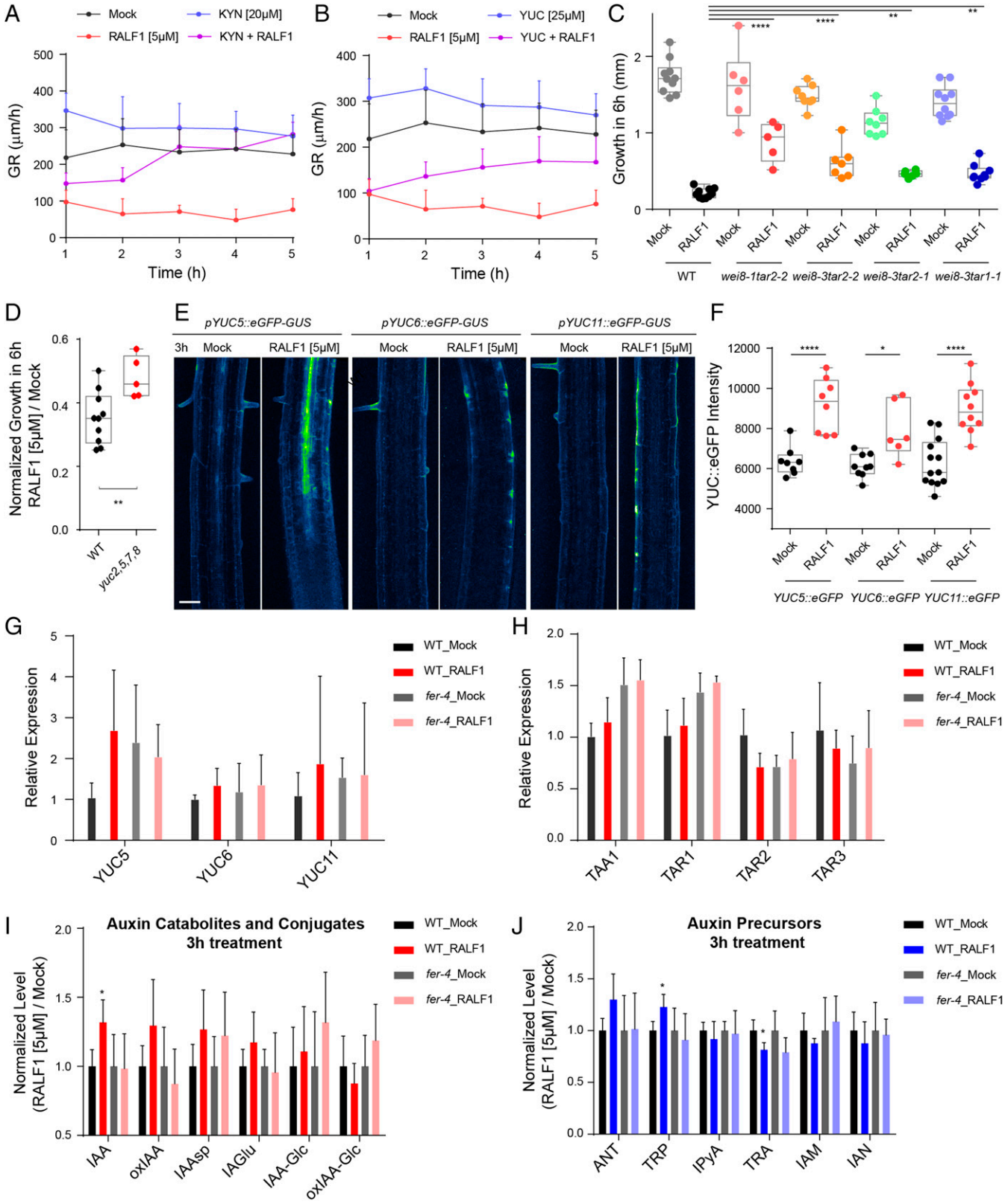

Fig. 4. RALF1-FER axis promotes auxin biosynthesis (*A* and *B*) Root GR of WT after 5 μM RALF1 treatment with auxin biosynthesis inhibitors [20 μM KYN (*A*) or 25 μM YUCA (*B*)] or Mock on vertical scanner. Before RALF1 treatment, WT roots were pretreated with inhibitors or Mock for 80 min. $n > 9$, mean + SD. $P < 0.0001$ between RALF1 and RALF1+KYN, and $P < 0.001$ between RALF1 and RALF1+YUCA, two-way ANOVA. (*C* and *D*) Root growth of auxin biosynthesis mutants *wei8-1tar2-2, wei8-3tar2-2, wei8-3tar2-1*, and *wei8-3tar1-1* (*C*) and *yuc2,5,7,8* (*D*) after 5 μM RALF1 for 6 h on vertical scanner. Box plot bars indicate the min and max value. $n > 5$. ****$P < 0.0001$; ***$P < 0.001$; **$P < 0.01$, one-way ANOVA. (*E* and *F*) Visualization (*E*) and quantification (*F*) of eGFP expressed under *YUC5*, *YUC6* and *YUC11* promoters after Mock or 5 μM RALF1 treatment for 3 h. *Z* stacks were taken in the late elongation zone, and a Green-Fire-Blue LUT was applied (*E*). Box plot bars indicate the min and max value. $n > 6$. ****$P < 0.0001$; *$P < 0.05$, one-way ANOVA (*F*). (*G* and *H*) qRT-PCR on the *YUCCA* (*G*) and *TAA1/TAR* (*H*) gene expression in roots of WT and *fer-4* with RALF1 (5 μM) or Mock treatment for 3 h. The expression level was normalized to PP2A. Mean of three biological replicates in three technical replicates + SD. (*I* and *J*) Auxin metabolites including auxin catabolites and conjugates (*I*) as well as precursors (*J*) after Mock or 5 μM RALF1 treatment for 3 h in WT or *fer-4* roots. Mean of five biological replicates with each containing 100 root tips + SD. *$P < 0.05$, one-way ANOVA.

RALF1 may induce an increase in auxin levels that contributes to root growth inhibition.

To understand how RALF1 induces auxin biosynthesis, we employed the reporter lines expressing eGFP-GUS under *YUC* native promoters. We observed an increased signal in the epidermal cells and stele of the late elongation zone of roots expressing *pYUC5::eGFP-GUS*, *pYUC6::eGFP-GUS*, and *pYUC11::eGFP-GUS* after treatment with 5 μM of RALF1 for 3 h (Fig. 4*E* and *F*). These data suggest that RALF1 induces auxin biosynthesis by up-regulating the transcription of *YUC*s. To examine whether these are FER-dependent, we analyzed the transcription level of *YUC5*, *-6*, and *-11* in *fer-4* comparing to WT after treatment with 5 μM of RALF1 for 3 h by qRT-PCR. Accordingly, we observed that RALF1-induced increase of *YUC5*, *-6*, and *-11* transcription depends on FER (Fig. 4*G*).

Next, we tested if TAAs are directly involved by qRT-PCR. Among all TAAs—including *TAA1*, *TAR1*, *TAR2*, and *TAR3*—no significant and consistent changes were observed (Fig. 4*H*). Furthermore, we examined the *pTAA1::TAA1-GFP* intensity in roots and found no change after RALF1 treatment (*SI Appendix*, Fig. S7*C*). These indicate that TAAs are not directly targeted by RALF1 signaling for regulation of auxin biosynthesis. Thus, the partial resistant phenotype to RALF1 in roots that are deficient in TAAs could be due to less substrate of the YUCCA enzyme.

To verify independently whether RALF1/FER signaling acts on auxin biosynthesis, we performed mass spectrometry analysis of auxin metabolites in root tips of the WT and *fer-4* treated with 5 μM of RALF1 or mock for 2 and 3 h. We found that RALF1 increased the levels of IAA, the major IAA catabolite oxIAA (only in 3 h), and the conjugates IAA-aspartate (IAAsp) and IAA-glutamate (IAGlu) in WT roots but less or not at all in *fer-4* mutants (Fig. 4*I* and *SI Appendix*, Fig. S7*D*). On the other hand, the direct IAA precursors indole-3-pyruvic acid (IPyA) was primarily decreased only in WT but not in *fer-4* after RALF1 treatment for 2 h (*SI Appendix*, Fig. S7*E*), following a recovery after 3 h (Fig. 4*J*). Other IAA precursors, such as indole-3-acetamide (IAM) and indole-3-acetonitrile (IAN), were slightly decreased in WT but less in *fer-4* (Fig. 4*J* and *SI Appendix*, Fig. S7*E*). The precursors in the earlier steps Trp was first decreased (*SI Appendix*, Fig. S7*E*) and then increased (Fig. 4*J*), with different changes in WT and *fer-4* mutants (Fig. 4*J* and *SI Appendix*, Fig. S7*E*). These indicate that RALF1 leads to a shift in auxin homeostasis from precursors to IAA to its catabolites and conjugates and that FER is involved.

Eventually, we confirm FER-mediated long-term response involving auxin by comparing the growth kinetics of *fer-4* after RALF1 treatment and cotreatment with IAA. The addition of IAA can restore the growth inhibition of *fer-4* (*SI Appendix*, Fig. S7 *F* and *G*). Taken together, these observations show that RALF1-FER triggers auxin biosynthesis up-regulation, contributing to sustained root growth inhibition.

Overall, the findings suggest that RALF1 triggers a biphasic FER-mediated root growth regulation, including 1) a phase of rapid and reversible growth inhibition through a net H^+ influx across the PM and 2) a phase of sustained growth inhibition mediated by canonical TIR1 auxin signaling via up-regulation of auxin biosynthesis (Fig. 5).

Discussion

RALF peptides are well-known signals triggering extracellular alkalinization and inhibiting root growth (4, 9). Despite the correlation between alkalinization and growth inhibition, their causal relationship remain largely unknown, as does underlying molecular mechanism. In this study, we used a microfluidic chip and vertical confocal microscopy to achieve simultaneous live imaging of root growth and apoplastic/cytosolic pH. We showed that in 1 min, RALF1 through its receptor FER triggers rapid growth inhibition and apoplast alkalinization (Fig. 1*C*, *E* and *F*) that is nontranscriptionally regulated (*SI Appendix*, Fig. S1*A*) and reversible (*SI Appendix*, Fig. S1*B*). Through external pH manipulation (Fig. 1*G–J*), we found that RALF1-FER–induced apoplast alkalinization leads to rapid and reversible growth inhibition. This resembles, but does not depend on, the rapid auxin regulation of root growth (Fig. 2*A* and *B*) (23). In turn, through an analysis of auxin signaling, transport and biosynthesis mutants, we uncovered a delayed, mechanistically different, RALF-FER response, mediating up-regulation of auxin biosynthesis leading to a sustained root growth inhibition (Fig. 4).

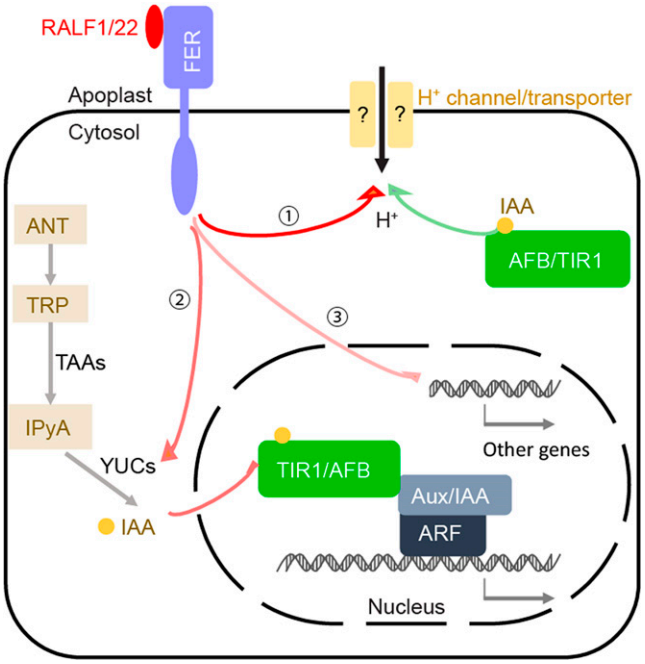

Fig. 5. Model for RALF1-induced root growth inhibition. Path 1: RALF1-FER triggers a rapid net H^+ influx across the PM, independent of PM H^+-ATPases. The resulting apoplast alkalinization mediates a rapid and reversible root growth inhibition. This path shares high similarity with but is independent of auxin-TIR1/AFB-mediated rapid root growth inhibition (shown in green arrow). Path 2: within about 1 h from stimulation, RALF1-FER promotes YUC expression and thus auxin biosynthesis to induce the canonical TIR1/AFB transcriptional pathway for sustained root growth inhibition. Path 3: other known transcriptional effects emanate from RALF1-FER.

RALF1-Triggered Rapid Apoplast Alkalinization and Root Growth Inhibition. We discovered that RALF1 induces an immediate net H^+ influx across the PM (Fig. 1*B–D*) in line with previously described effects of RALF33 and RALF36 (34). Regarding the mechanism, by which RALF-FER signaling can mediate net H^+ influx, it has been suggested that RALF1 may lead to the deactivation of PM H^+-ATPase AHA2 (9). However, it is unclear whether PM H^+-ATPases in *A. thaliana* are indeed deactivated responding to RALF1 and how much this contributes to rapid alkalinization (14). To study the role of PM H^+-ATPase during RALF1-induced root growth inhibition, we examined the mutants in PM H^+-ATPases and the mutants that had different PM H^+-ATPase levels or activity (*SI Appendix*, Fig. S3). Available *aha* mutants showed normal

growth reduction (*SI Appendix*, Fig. S3 *J* and *L*), except for the *AtTAS1c-AHA* mutants, which were hypersensitive to RALF1 within 5 h (*SI Appendix*, Fig. S3*K*). In addition, *tmk* mutants which have low AHA activity levels, for example, *tmk1-1*, *tmk1,2*, and *tmk1,4* roots were also hypersensitive to RALF1 for 1 to 5 h (*SI Appendix*, Fig. S3 *C–G*). Similarly for the rapid response, RALF1 led to more alkalinization in the apoplast of *tmk1,2* (*SI Appendix*, Fig. S3*B*). These results do not support a direct role of TMK and AHA in RALF-mediated apoplast alkalinization, although we cannot exclude the presence of residual activities in the used genotypes. Presumably, an unknown H^+ channel or transporter would be involved as implied also in the auxin-mediated apoplast alkalinization. Whether the RALF1-FER and auxin-TIR/AFB signaling are converging on the same mechanism of the H^+ influx or leakage requires further investigation.

RALF1-Triggered Sustained Growth Inhibition by Induction of Auxin Biosynthesis. Our tracking the kinetics of root growth after RALF1 application combined with analysis of auxin signaling-deficient mutants revealed a biphasic growth response. The roots of auxin mutants responded normally to RALF1 treatment within the first hour but then displayed a strong resistance (Fig. 2 and *SI Appendix*, Fig. S4). This phenomenon resulted from a delayed activation of auxin signaling (Fig. 3) through RALF1-FER–induced up-regulation of auxin biosynthesis (Fig. 4).

In summary, we discovered that RALF1-FER triggers a biphasic root growth regulation that includes: 1) a phase of rapid and reversible growth inhibition caused by a net H^+ influx, and 2) a phase of sustained growth inhibition mediated by activated auxin biosynthesis and auxin signaling (Fig. 5). This biphasic growth regulation by RALF signaling peptides enables both immediate and sustained growth and developmental adaptation in response to environmental changes.

Materials and Methods

Plant Materials and Growth Conditions. All *A. thaliana* mutants and transgenic lines used are in Columbia-0 (Col-0) background. PM-Cyto marker line (33), *fer-4* (12), complemented line *pFER:FER-GFP/fer-4* (12), *the1-1* (31), *tir1-1afb2-1afb3-1* (45), *HS::axr3-1* (46), *pYUC5::eGFP-GUS*, *pYUC6::eGFP-GUS*, *pYUC11::eGFP-GUS* (47), *R2DII* (39), *DR5rev::GFP* (48), *DR5::LUC* (40), *tmk1-1* (SALK_016360) (49), *tmk4-1* (GABI_348E01) (49), *tmk1-1tmk4-1* (49), *ost2-3D* (50), *p35S::SAUR19-GFP* (37), *pin2* (55), *pin3,4,7* (55), and *pTAA1::TAA1-GFP* (26) were kindly shared by the authors. The *herk1-1* (SALK_008043), *aha2-4 (SALK_082786.46.35.x)*, and *aha1-7* (SALK_016325) were ordered from the Nottingham *Arabidopsis* Stock Center. Two independent lines *AtTAS1c-AHA#2* and *#4* were generated as described previously (23).

Seeds were surface-sterilized by chlorine gas, sown on half-strength Murashige and Skoog (1/2 MS) medium supplemented with 1% (wt/vol) sucrose and 0.8% (wt/vol) phyto agar (pH 5.9), stratified in the dark at 4 °C for 2 d and then grown vertically at 21 °C with a long-day photoperiod (16-h light/8-h dark). Light sources used were Philips GreenPower LED production modules [in deep red (660 nm)/far-red (720 nm)/blue (455 nm) combination, Philips], with a photon density of 140.4 μmol/m^2/s ± 3%. Four- to 5-d-old seedlings were used.

Microfluidics. The microfluidic vRootchip was used to analyze rapid changes in root tip growth and apoplastic pH in real-time. The manufacturing of the chip, sample preparation procedure, and data analysis of root tip growth were performed as described previously (21, 23). Next, 1/4 MS + 0.1% sucrose was used as a basal medium during operation to avoid contamination. For one vRootchip, a maximum of eight samples were used. When comparing two genotypes, three to four seedlings were used for each genotype and mounted in alternating channels to minimize the time difference between imaging the two genotypes. For each root, one region of interest (ROI) containing early elongating epidermal cells and the other ROI covering the root tip were imaged. As these two ROIs were captured sequentially, the apoplastic pH and the growth of the same root were imaged close to simultaneously with an in-house established vertical Zeiss LSM 800 confocal microscope (32). Note that RALF peptide in a longer time coats the channels and cannot be washed out in vRootchip; therefore, washout experiments were done by transferring RALF-incubated seedlings to fresh agar block containing basic medium.

TipTracker Assay. TipTracker assay was used as a complementary approach to perform confocal imaging for long time periods up to hours, as well as RALF washout experiments. Next, 1/2 MS agar medium with indicated treatments or mock were prepared and solidified. A slice of this agar block was cut and 4- to 5-d-old seedlings placed on top before transferring to a Lab-Tek Chambered Coverglass. The chamber was mounted onto the vertical Zeiss LSM 800 confocal microscope (32). Imaging and analysis of root growth were done with the TipTracker scripts described previously (32).

Vertical Scanner Growth Assay. As a high-throughput method of growth analysis, we used a vertical flatbed scanner (Epson perfection V370) (35) with slots for Petri dishes containing 1/2 MS medium with treatments as indicate. Automatic scanning at 1,200 dpi every hour using the AutoIt script was described previously (51). The resulting image series were analyzed using StackReg stabilization and the Manual Tracking plugin in ImageJ.

Imaging and Measuring Apoplastic pH with HPTS Dye. For imaging, 1 mM HPTS dye (Thermo Scientific 6358-69-6, dissolved in ddH_2O) was applied in TipTracker and vRootchip assays. Imaging was performed on the vertical Zeiss LSM 800 confocal microscope (32). Fluorescent signals for protonated HPTS (excitation 405 nm, emission 514 nm, visualized in red) and deprotonated HPTS (excitation 488 nm, emission 514 nm, visualized in green) were detected with a 20×/0.8 air objective. Image analysis was performed on a cropped region of elongating epidermis cells using a previously described ImageJ macro with batch processing modification (27). The relative pH value is calculated as the background-subtracted intensity of the deprotonated intensity divided by that of the protonated intensity to represent the relative pH. Note that the relative pH value was not transformed to the absolute pH values, which requires the generation of a calibration curve for each experiment.

Imaging and Measuring Cytosolic pH with the PM-Cyto Reporter Line. Real-time imaging of the cytosolic pH near the PM was done by using the PM-Cyto reporter in vRootchip on the vertical confocal microscope. Sequential illumination at 488 and 405 nm with emission 514 nm for both, corresponding to two absorption peaks of pHluorin, were taken with a 20×/0.8 air objective. For each root in vRootchip, two ROIs were tracked over time, with one containing the elongating epidermal cell for measuring cytosolic pH and one containing the root tip for measuring root growth rate. Image analysis was performed similarly to the HPTS analysis described above.

Auxin Signaling Evaluation. Four-day-old seedlings of *R2DII*, *DR5rev::GFP*, or *DR5::LUC* line were used. The former two were transferred to 1/2 MS agar blot containing treatments as indicated and immediately mounted on the vertical confocal microscope for live imaging. The *DR5::LUC* seedlings were transferred to 1/2 MS agar blot medium containing treatments as indicated and immediately drops of 1 mM D-luciferin in 1/2 MS liquid medium were applied on top of roots. These samples were transferred to a dark box (51), and luminescence was captured every two minutes using a Photometrics Evolve 512 EMCCD camera equipped with a 17-mm fixed lens/0.95 and an additional 125-mm lens. The EMCCD multiplier gain was 150 and the exposure time was 90 s.

Imaging and Measuring Auxin Biosynthesis Reporters. Four-day-old seedlings of *pYUC5::eGFP-GUS*, *pYUC6::eGFP-GUS*, *pYUC11::eGFP-GUS*, *pTAA1::TAA1-GFP* were transferred to 1/2 MS agar blot containing treatments of Mock or RALF1(5 μM). The former three were imaged after treatment for 3 h. The *pTAA1::TAA1-GFP* roots were tracked from 16 min to about 2 h. The late-elongation epidermal cells with eGFP signal were imaged at excitation 488 nm and emission 509 nm on a Zeiss LSM 800 inverted confocal microscope with a Plan-Apochromat 20×/0.8 air objective.

Quantitative RT-PCR. RNA was extracted from 4-d-old roots with the RNeasy Plant Mini kit (Qiagen), with three biological replicates for each

genotype. Two micrograms of RNA were used for cDNA synthesis (Qiagen). Samples were pipetted in three technical replicates using an automated JANUS Workstation (PerkinElmer) and measured on a Roche Real-Time PCR LightCycler 480 using Luna Universal qPCR Master Mix (New England Biolabs, M3003S). Primers used to assess gene expression are listed in *SI Appendix*, Table S1. Expression levels were normalized to those for protein phosphatase 2A (PP2A).

Mass Spectrometry Analysis of Auxin Metabolites. Concentrations of IAA and different IAA metabolites (precursors, conjugates, and catabolites) were measured using liquid chromatography-tandem mass spectrometry (Agilent Instruments) as described by Novák et al. (52). Four-day-old seedlings were treated with Mock or RALF1 (5 μM) for 2 or 3 h. Afterward, five replicates of 100 root tips per condition were cut and flash-frozen in liquid nitrogen. The extraction procedure and the further analysis by using a Pegasus III gas chromatography/time-of-flight mass spectrometer (Leco) essentially follow (53). The chromatograms were processed with in-house developed scripts (54).

Statistical Analysis. All graphs were generated using GraphPad Prism 6. For statistical analysis of vRootchip data, two-way ANOVA was performed for the entire time of the *x* axis. One-way ANOVA assays were used for others. Asterisks indicate significant differences on all graphs with ns = $P > 0.05$, *$P \leq 0.05$, **$P \leq 0.01$, ***$P \leq 0.001$ and ****$P \leq 0.0001$.

Data Availability. All study data are included in the main text and/or *SI Appendix*.

ACKNOWLEDGMENTS. We thank Sarah M. Assmann, Kris Vissenberg, and Nadine Paris for kindly sharing seeds; Matyáš Fendrych for initiating this project and providing constant support; Lukas Fiedler for revising the manuscript; and Huibin Han and Arseny Savin for contributing to genotyping. This work was supported by the Austrian Science Fund (FWF) I 3630-B25 (to J.F.) and the Doctoral Fellowship Progrmme of the Austrian Academy of Sciences (to L.L.) We also acknowledge Taif University Researchers Supporting Project TURSP-HC2021/02 and funding "Plants as a tool for sustainable global development (no. CZ.02.1.01/0.0/0.0/16_019/0000827)."

Author affiliations: [a]Beijing Key Laboratory of Development and Quality Control of Ornamental Crops, Department of Ornamental Horticulture, College of Horticulture, China Agricultural University, 100193 Beijing, China; [b]Institute of Science and Technology Austria, 3400 Klosterneuburg, Austria; [c]Department of Biotechnology, College of Science, Taif University, 21944 Taif, Saudi Arabia; and [d]Laboratory of Growth Regulators, Faculty of Science, Palacký University and Institute of Experimental Botany of the Czech Academy of Sciences, 78371 Olomouc, Czech Republic

1. G. Arsuffi, S. A. Braybrook, Acid growth: An ongoing trip. *J. Exp. Bot.* **69**, 137–146 (2018).
2. M. Du, E. P. Spalding, W. M. Gray, Rapid Auxin-Mediated Cell Expansion. *Annu. Rev. Plant Biol.* **71**, 379–402 (2020).
3. G. Pearce, D. S. Moura, J. Stratmann, C. A. Ryan Jr, RALF, a 5-kDa ubiquitous polypeptide in plants, arrests root growth and development. *Proc. Natl. Acad. Sci. U.S.A.* **98**, 12843–12847 (2001).
4. M. Haruta, G. Monshausen, S. Gilroy, M. R. Sussman, A cytoplasmic Ca^{2+} functional assay for identifying and purifying endogenous cell signaling peptides in Arabidopsis seedlings: Identification of AtRALF1 peptide. *Biochemistry* **47**, 6311–6321 (2008).
5. L. Campbell, S. R. Turner, A comprehensive analysis of RALF proteins in green plants suggests there are two distinct functional groups. *Front. Plant Sci.* **8**, 37 (2017).
6. J. Cao, F. Shi, Evolution of the RALF gene family in plants: Gene duplication and selection patterns. *Evol. Bioinform.* **8**, 271–292 (2012).
7. S. Masachis *et al.*, A fungal pathogen secretes plant alkalinizing peptides to increase infection. *Nat. Microbiol.* **1**, 16043 (2016).
8. E. Thynne *et al.*, Fungal phytopathogens encode functional homologues of plant rapid alkalinization factor (RALF) peptides. *Mol. Plant Pathol.* **18**, 811–824 (2017).
9. M. Haruta, G. Sabat, K. Stecker, B. B. Minkoff, M. R. Sussman, A peptide hormone and its receptor protein kinase regulate plant cell expansion. *Science* **343**, 408–411 (2014).
10. A. Y. Cheung, H.-M. Wu, THESEUS 1, FERONIA and relatives: A family of cell wall-sensing receptor kinases? *Curr. Opin. Plant Biol.* **14**, 632–641 (2011).
11. P. Liu, M. Haruta, B. B. Minkoff, M. R. Sussman, Probing a plant plasma membrane receptor kinase's three-dimensional structure using mass spectrometry-based protein footprinting. *Biochemistry* **57**, 5159–5168 (2018).
12. D. Chakravorty, Y. Yu, S. M. Assmann, A kinase-dead version of FERONIA receptor-like kinase has dose-dependent impacts on rosette morphology and RALF1-mediated stomatal movements. *FEBS Lett.* **592**, 3429–3437 (2018).
13. M. Haruta, V. Gaddameedi, H. Burch, D. Fernandez, M. R. Sussman, Comparison of the effects of a kinase-dead mutation of FERONIA on ovule fertilization and root growth of Arabidopsis. *FEBS Lett.* **592**, 2395–2402 (2018).
14. M. R. Blackburn, M. Haruta, D. S. Moura, Twenty years of progress in physiological and biochemical investigation of RALF peptides. *Plant Physiol.* **182**, 1657–1666 (2020).
15. K. Dressano *et al.*, BAK1 is involved in AtRALF1-induced inhibition of root cell expansion. *PLoS Genet.* **13**, e1007053 (2017).
16. W. F. Campos *et al.*, *Arabidopsis thaliana* rapid alkalinization factor 1-mediated root growth inhibition is dependent on calmodulin-like protein 38. *J. Biol. Chem.* **293**, 2159–2171 (2018).
17. J. Friml, Fourteen stations of auxin. *CSH Perspect. Biol.* **14**, a039859 (2021).
18. K. Mashiguchi *et al.*, The main auxin biosynthesis pathway in Arabidopsis. *Proc. Natl. Acad. Sci. U.S.A.* **108**, 18512–18517 (2011).
19. J. Petrásek, J. Friml, Auxin transport routes in plant development. *Development* **136**, 2675–2688 (2009).
20. M. Lavy, M. Estelle, Mechanisms of auxin signaling. *Development* **143**, 3226–3229 (2016).
21. M. Fendrych *et al.*, Rapid and reversible root growth inhibition by TIR1 auxin signalling. *Nat. Plants* **4**, 453–459 (2018).
22. S. M. Dubey, N. B. C. Serre, D. Oulehlová, P. Vittal, M. Fendrych, No time for transcription–Rapid auxin responses in plants. *Cold Spring Harb. Perspect. Biol.* **13**, 039891 (2021).
23. L. Li *et al.*, Cell surface and intracellular auxin signalling for H^+ fluxes in root growth. *Nature* **599**, 273–277 (2021).
24. M. Cao *et al.*, TMK1-mediated auxin signalling regulates differential growth of the apical hook. *Nature* **568**, 240–243 (2019).
25. W. Lin *et al.*, TMK-based cell-surface auxin signalling activates cell-wall acidification. *Nature* **599**, 278–282 (2021).
26. Q. Wang *et al.*, A phosphorylation-based switch controls TAA1-mediated auxin biosynthesis in plants. *Nat. Commun.* **11**, 679 (2020).
27. E. Barbez, K. Dünser, A. Gaidora, T. Lendl, W. Busch, Auxin steers root cell expansion via apoplastic pH regulation in *Arabidopsis thaliana*. *Proc. Natl. Acad. Sci. U.S.A.* **114**, E4884–E4893 (2017).
28. Q. Dong, Z. Zhang, Y. Liu, L. Z. Tao, H. Liu, FERONIA regulates auxin-mediated lateral root development and primary root gravitropism. *FEBS Lett.* **593**, 97–106 (2019).
29. E. Li, G. Wang, Y. L. Zhang, Z. Kong, S. Li, FERONIA mediates root nutating growth. *Plant J.* **104**, 1105–1116 (2020).
30. M. Yu *et al.*, The RALF1-FERONIA interaction modulates endocytosis to mediate control of root growth in *Arabidopsis*. *Development* **147**, dev189902 (2020).
31. M. Gonneau *et al.*, Receptor kinase THESEUS1 is a rapid alkalinization factor 34 receptor in Arabidopsis. *Curr. Biol.* **28**, 2452–2458.e2454 (2018).
32. D. von Wangenheim *et al.*, Live tracking of moving samples in confocal microscopy for vertically grown roots. *eLife* **6**, e26792 (2017).
33. A. Martinière *et al.*, Uncovering pH at both sides of the root plasma membrane interface using noninvasive imaging. *Proc. Natl. Acad. Sci. U.S.A.* **115**, 6488–6493 (2018).
34. S. K. Gjetting *et al.*, Evidence for multiple receptors mediating RALF-triggered Ca^{2+} signaling and proton pump inhibition. *Plant J.* **104**, 433–446 (2020).
35. Y. Zhang, L. Li, J. Friml, Evaluation of gravitropism in non-seed plants. *Methods Mol. Biol.* **2368**, 43–51.
36. A. Carbonell *et al.*, New generation of artificial MicroRNA and synthetic trans-acting small interfering RNA vectors for efficient gene silencing in Arabidopsis. *Plant Physiol.* **165**, 15–29 (2014).
37. A. K. Spartz *et al.*, SAUR inhibition of PP2C-D phosphatases activates plasma membrane H^+-ATPases to promote cell expansion in Arabidopsis. *Plant Cell* **26**, 2129–2142 (2014).
38. K. Hayashi *et al.*, Rational design of an auxin antagonist of the $SCF^{(TIR1)}$ auxin receptor complex. *ACS Chem. Biol.* **7**, 590–598 (2012).
39. C.-Y. Liao *et al.*, Reporters for sensitive and quantitative measurement of auxin response. *Nat. Methods* **12**, 207–210 (2015).
40. M. A. Moreno-Risueno *et al.*, Oscillating gene expression determines competence for periodic Arabidopsis root branching. *Science* **329**, 1306–1311 (2010).
41. L. Abas *et al.*, Naphthylphthalamic acid associates with and inhibits PIN auxin transporters. *Proc. Natl. Acad. Sci. U.S.A.* **118**, e2020857118 (2021).
42. W. He *et al.*, A small-molecule screen identifies L-kynurenine as a competitive inhibitor of TAA1/TAR activity in ethylene-directed auxin biosynthesis and root growth in Arabidopsis. *Plant Cell* **23**, 3944–3960 (2011).
43. T. Nishimura *et al.*, Yucasin is a potent inhibitor of YUCCA, a key enzyme in auxin biosynthesis. *Plant J.* **77**, 352–366 (2014).
44. N. Morffy, L. C. Strader, Old town roads: Routes of auxin biosynthesis across kingdoms. *Curr. Opin. Plant Biol.* **55**, 21–27 (2020).
45. N. Dharmasiri *et al.*, Plant development is regulated by a family of auxin receptor F box proteins. *Dev. Cell* **9**, 109–119 (2005).
46. K. Knox, C. S. Grierson, O. Leyser, AXR3 and SHY2 interact to regulate root hair development. *Development* **130**, 5769–5777 (2003).
47. H. S. Robert *et al.*, Local auxin sources orient the apical-basal axis in Arabidopsis embryos. *Curr. Biol.* **23**, 2506–2512 (2013).
48. J. Friml *et al.*, Efflux-dependent auxin gradients establish the apical-basal axis of Arabidopsis. *Nature* **426**, 147–153 (2003).
49. R. Huang *et al.*, Noncanonical auxin signaling regulates cell division pattern during lateral root development. *Proc. Natl. Acad. Sci. U.S.A.* **116**, 21285–21290 (2019).
50. S. Yamauchi *et al.*, The plasma membrane H^+-ATPase AHA1 plays a major role in stomatal opening in response to blue light. *Plant Physiol.* **171**, 2731–2743 (2016).
51. L. Li, S. F. G. Krens, M. Fendrych, J. Friml, Real-time analysis of auxin response, cell wall pH and elongation in *Arabidopsis thaliana* Hypocotyls. *Bio Protoc.* **8**, e2685 (2018).
52. O. Novák *et al.*, Tissue-specific profiling of the *Arabidopsis thaliana* auxin metabolome. *Plant J.* **72**, 523–536 (2012).
53. J. Gullberg, P. Jonsson, A. Nordström, M. Sjöström, T. Moritz, Design of experiments: An efficient strategy to identify factors influencing extraction and derivatization of *Arabidopsis thaliana* samples in metabolomic studies with gas chromatography/mass spectrometry. *Anal. Biochem.* **331**, 283–295 (2004).
54. P. Jonsson *et al.*, High-throughput data analysis for detecting and identifying differences between samples in GC/MS-based metabolomic analyses. *Anal. Chem.* **77**, 5635–5642 (2005).
55. Y. Zhang, L. Rodriguez, L. Li, X. Zhang, J. Friml, Functional innovations of PIN auxin transporters mark crucial evolutionary transitions during rise of flowering plants. *Sci. Adv.* **6**, eabc8895 (2020).